ON THE DIURNAL EVOLUTION OF ISOPRENE AND THE HYDROXYL RADICAL OVER TROPICAL FORESTS

Jordi Vilà-Guerau de Arellano[1],[*] Edward G. Patton[2], Thomas Karl[2],
Kees van den Dries[1], Mary C. Barth[2], John J. Orlando[2]

[1]Meteorology and Air Quality Section, Wageningen University, Wageningen, The Netherlands
[2]National Center for Atmospheric Research, Boulder, CO

1. Introduction

The reactivity of key compounds like ozone, isoprene and the hydroxyl radical is controlled by physical and chemical processes occurring in the lower part of the troposphere, namely the atmospheric boundary layer (ABL), where these species can directly interact with the land surface. During a diurnal cycle, the ABL experiences a large height variation in response to time-dependent buoyancy forcing (ranging from heights as small as 100 m or smaller at night up to more than 2 km during midday). This height variation has two key implications for ABL chemistry: 1) as the ABL grows during the morning, free tropospheric (FT) air is entrained into the ABL which is typically characterized by concentrations of atmospheric compounds different than those within the ABL, and 2) surface-emitted or entrained species are mixed into a growing volume throughout the day and then into a smaller volume after the buoyancy forcing shuts down and the convective boundary layer collapses. The entrainment process is often overlooked in studies focusing on soil and vegetation exchanges of reactants and turbulent mixing within the atmospheric surface layer. Therefore, the aim here is to quantify the importance of ABL-growth and the subsequent FT-ABL exchange relative to surface sources/sinks.

By combining observations taken during the Tropical Forest and Fire Emission Experiment (TROFFEE) campaign (Karl et al., 2007; Yokelson et al., 2008) and numerical experiments carried out using the large-eddy simulation technique (Heus et al., 2010) and mixed-layer theory (Vilà-Guerau de Arellano et al., 2009), we study the interplay between turbulent dynamics and the O_3-NO_x-VOC-HO_x chemistry in the Amazonian boundary layer. The reasons to select Amazonia are fourfold: 1) the chemistry is characterized by high biogenic emissions and the role of dynamics is not yet well understood (Butler et al., 2008; Ganzeveld et al., 2008; Pugh et al., 2009), 2) tropical systems are globally significant in regulating atmospheric composition (Karl et al.,

2007; Lelieveld et al., 2008), 3) the Amazon is undergoing rapid changes in surface-vegetation characteristics through deforestation and Amazonian ABL dynamics and chemistry is potentially very sensitive to these modifications (*e.g.,* Fan et al., 1990; Keller et al., 1991), and 4) disagreements between measured and modeled OH have been observed, and a variety of different chemical reaction pathways that form and destroy OH have been proposed (*e.g.,* Lelieveld et al., 2008; Peeters et al., 2009).

The role of entrainment on heat and moisture budgets has been previously investigated for clear (*e.g.,* Tennekes, 1973) and stratocumulus boundary layers (*e.g.,* Lilly, 1968). Large-eddy simulation has enabled investigations into the dynamics determining entrainment in free convective situations (Sullivan et al., 1998; Jonker et al., 1999) and into the influence of wind shear on entrainment (Pino et al., 2003; Conzemius and Fedorovich, 2006). For moisture and carbon dioxide, observation (Davis et al., 1994; Casso-Torralba et al., 2008) and modeling (Martin et al., 1988; Vilà-Guerau de Arellano et al., 2004; van Heerwaarden et al., 2009) studies suggest that entrainment is as important as the surface process in estimating the diurnal budget of water vapor and CO_2. For atmospheric reactants, Martin et al. (1988) suggested the importance of the FT-ABL exchange in regulating the diurnal cycle of reactants in the Amazonian region, however to our knowledge no further attempt has been made to quantify the role of entrainment on diurnal reactant variation.

The research in this current manuscript therefore aims to determine which processes control the diurnal evolution of reactants in the O_3-NO_x-VOC-HO_x system, and consequently to determine which processes need to be included in boundary layer parameterization schemes to adequately reproduce their diurnal characteristics. Since we have observations of isoprene and its major by-products available from TROFFEE, we mainly focus our analysis on those species but extend that analysis to the OH radical due to its oxidizing relevance in Amazonia (Zimmerman et al., 1988; Guenther et al., 1996; Fuentes et al., 2000; Karl et al., 2007; Lelieveld et al., 2008).

[*]*Corresponding address:*, Jordi Vilà-Guerau de Arellano, Meteorology and Air Quality Section, P.O. Box 47, Wageningen University, 6700 AA Wageningen, The Netherlands, jordi.vila@wur.nl

Systematic numerical experiments are carried out to determine and quantify the roles of: 1) FT-ABL exchange, 2) isoprene surface emission, and 3) OH reactivity in modulating reactant diurnal evolution. In consequence, these numerical experiments enable us to establish the different contribution from each process and to determine their importance at different stages of the boundary layer evolution. A final investigation studies the relationship between surface isoprene emission flux and the atmospheric mixing ratio for other observational campaigns in the tropics.

This study also permits assessment of the turbulence-resolving large-eddy simulation technique for studying complex chemical systems and establishes expected relationships between LES and predictions using zeroth-order mixed-layer (MXL) theory applied to ABL chemistry. Models based on MXL theory permit incorporation of surface and entrainment flux relationships into a simple conceptual model of boundary layer dynamics and its interaction with chemistry while maintaining similar computational expense to box model simulations. The mixed-layer model representation of the convective boundary layer is similar to parameterizations implemented in large-scale chemistry-transport models; this close relationship consequently enables identification of the key processes needing inclusion or improvement within such boundary layer schemes.

The structure of this article is as follows: Section 2. describes the design of the numerical experiments and the sensitivity studies. The dynamical and chemical evolution of the boundary layer obtained through large-eddy simulation and through the mixed-layer model are evaluated against observations and discussed in Section 3.. Section 4. focuses on determining and comparing the main processes driving diurnal variability of isoprene and the hydroxyl radical, namely: 1) FT-ABL exchange, 2) surface emissions, and 3) reactivity. Section 5. extends this investigation by looking at the relationship between the isoprene emission and atmospheric mixing ratio by analyzing data collected during a variety of Amazonian observational campaigns characterized by different biogenic surface fluxes. Section 6. closes the paper by summarizing the main conclusions and emphasizing the need for an appropriate balance between ABL dynamics and chemistry when investigating ABL chemistry from either a modeling and an observational perspective.

2. Design of the numerical experiment

2.1 Observations

Our numerical experiments are designed to mimic the meteorology and chemistry observed during TROFFEE which took place 60 km NNW of Manaus in Central Amazonia (2.612 S, 60.91 W) during the dry season between 14 and 29 September 2004 (Karl et al., 2007). The Manaus region is largely not influenced by biomass burning due to the vast expanse of surrounding undisturbed forest upwind. TROFFEE focused mainly on measuring trace atmospheric compounds, but also included observations of potential temperature and sensible heat flux. These surface fluxes and upper atmospheric conditions observed during TROFFEE were combined with observations from previous Amazonian ABL studies (Martin et al., 1988; Garstang et al., 1990; Betts and Jacob, 2002) to create a generic atmospheric situation reproducing a typical Amazonian boundary layer undisturbed by large-scale forcing. Similarly, hourly-averaged atmospheric chemistry observations from the 15-day TROFFEE campaign are used to impose time-evolving surface isoprene and nitric oxide emission fluxes.

2.2 Atmospheric representation

The study is based on the simulations carried out by two numerical tools: 1) the Dutch Atmospheric Large-Eddy Simulation (DALES) (Heus et al., 2010; Vilà-Guerau de Arellano et al., 2005), and 2) a much simpler model based on mixed-layer theory (MXLCH) (Tennekes, 1973; Vilà-Guerau de Arellano et al., 2009). The large-eddy simulation technique solves the filtered three-dimensional thermodynamic equations and conservation equation for reactive species, and as a result produces three-dimensional time-evolving fields. In convective boundary layers, LES explicitly reproduces approximately 90% of the energy contained in the turbulent eddies. Therefore it is also able to account for the influence of large-scale turbulent mixing on chemical reactivity and on the entrainment process.

Although the LES is highly accurate, it is also computationally expensive. The MXLCH model allows for a less expensive means to reasonably represent key ABL processes. The MXLCH model assumes horizontal homogeneity and perfectly mixed convective boundary layer characteristics resulting in a one-dimensional representation producing vertical profiles which are constant with height within the mixed layer. Based on these characteristics, the governing equations of this conceptual model are therefore obtained by the vertical integration of the one-dimensional thermodynamic equations and conservation equation for reactive species.

A relevant aspect to appreciate is that the MXLCH model is very similar to a box model where heat/moisture/reactant sources can be introduced in to the box; these sources/sinks might be time-dependent but are generally specified *a priori* and are intended to mimic all possible sources/sinks to the box. MXLCH also includes this imposed source but that imposed source is in-

Boundary layer properties

Initial boundary layer height, h [m]	200
Large scale subsidence velocity, w_s [m s^{-1}]	0
Imposed geostrophic wind, (U_g, V_g) [m s^{-1}]	(0, 0)
Surface roughness length, $z_\circ$ [m]	0.035

Heat

Surface sensible heat flux (from 0725 to 1525 LT) [K m s^{-1}]	$\overline{w\theta}_s = 0.19 \sin\left(\frac{\pi(t-8100)}{28800}\right)$
Entrainment to surface sensible flux ratio, β_{MXLCH}	$(\overline{w\theta}_v)_e / (\overline{w\theta}_v)_s = -0.2$
Potential temperature profile: [K]	

$z < 200.0$ m	299.0
200.0 m $< z < 212.5$ m	300.0
$z > 212.5$ m	$300.0 + 6 \cdot 10^{-3} \cdot z$

Moisture

Latent heat flux (from 0600 to 1650 LT) [g kg^{-1} m s^{-1}]	$\overline{wq}_s = 0.13 \sin\left(\frac{\pi(t-3600)}{37800}\right)$
Specific moisture profile: [g kg^{-1}]	

$z < 200.0$ m	15.0
200.0 m $< z < 212.5$ m	15.0
$z > 212.5$ m	10.0

Table 1: The initial and prescribed values used for the large-eddy simulation (DALES) and the mixed-layer model (MXLCH) numerical experiments. All initial conditions are imposed at 0500 LT. t is the time in [s]. The subscripts s and e indicate values at the surface and the entrainment zone, respectively.

terpreted solely as a surface source into a perfectly mixed box. Additionally, MXLCH incorporates a simple mechanism by which the boundary layer (the box) can grow vertically through the action of parameterized buoyancy-driven turbulent motions eating away at an infinitesimally sharp gradient at the top of the boundary layer (the box) thereby exchanging heat/moisture/reactants across that interface. If the mixing ratio above the box is higher(lower) than that within the box then there is an additional source(sink) of that quantity to(from) the box, where the magnitude of that source(sink) is assumed to be proportional to the growth rate of the box and the magnitude of the mixing ratio gradient across the interface. See Vilà-Guerau de Arellano et al. (2009) for further details. Although MXLCH represents entrainment in this extremely simplified fashion, it captures the essential interplay between surface forcing, boundary layer dynamics, entrainment zone variations and free tropospheric conditions that is not captured in box model simulations.

While the fluid mechanics between DALES and MXLCH differ, they share an identical two-step chemical solver (Verwer, 1994; Verwer and Simpson, 1995). This two-step chemical solver is an implicit method with second-order accuracy based on the two-step back-ward differentiation formula which is able to adjust the time step depending on the chemical reaction rate (Vilà-Guerau de Arellano et al., 2009; Heus et al., 2010).

The LES calculations are carried out using a 12800 m × 12800 m horizontal and a 2550 m vertical domain resolved by 128 × 128 × 128 grid points. Periodic boundary conditions are imposed in the horizontal directions, and Monin-Obukhov similarity theory is used to relate quantities at the first grid point to the imposed surface fluxes at the ground. MXLCH uses the identical initial conditions and surface emissions as are imposed in the LES-experiments.

Fifteen-day averaged TROFFEE observations are prescribed as initial and boundary conditions in the numerical experiments (Table 1). The geostrophic wind is 0 m s^{-1} (*i.e.,* local free convective conditions). The roughness length is 0.035 m. We do not prescribe any large scale forcing (zero horizontal heat or moisture, no subsidence, nor radiative tendencies). The simulation begins at 0500 local time (LT) and it lasts 13 hours. With this numerical design, we are able to reproduce the average diurnal variability at the TROFFEE site (sunrise is at 0600 LT and sunset occurs at 1800 LT).

Amazonian ABL's are typically characterized by a

warm and moist ABL capped by a free troposphere which is close to being conditionally unstable (Garstang et al., 1990; Betts and Jacob, 2002). These conditions favor the formation of shallow cumulus during the day, which significantly complicates the relationships between surface/entrainment fluxes and mid-ABL concentrations. To simplify the interpretation of our results, we chose not to permit cloud formation in our simulations by not allowing condensation.

2.3 Chemistry representation

Simulating the interactions between turbulence and chemistry is computationally intensive. We therefore chose an approach that balances the costs between dynamics and chemistry while minimizing any compromise for either component. We select a chemical mechanism which reproduces the essential components of the O_3-NO_x-VOC-HO_x system while allowing a series of LES-experiments with sufficient numerical resolution to reproduce the atmospheric fluid dynamics. The chemical mechanism is described in Table 2. In short, we use a highly condensed gas-phase mechanism describing the basic features of isoprene-NO_x-O_3 chemistry in the remote tropical atmosphere. For instance, all first generation products of isoprene oxidation [mainly methyl vinyl ketone (MVK) and methacrolein (MACR)] are lumped into a single species, which is called MVK. Thus, in comparisons made later in the paper, only semi-quantitative agreement should be expected between modeled (lumped) "MVK", which is assumed to be formed in 100% yield in (R13), and measured MVK (which from the PT-RMS is actually the sum of MVK and MACR and are in reality formed in 60% yield (Tuazon and Atkinson, 1990)).

All the reactions rates are specified in Table 2, except for R15, where we assume the following reaction rate:

$$k = (k_1 + k_2) \cdot k_3 \qquad (1)$$

where,

$$k_1 = 2.2 \cdot 10^{-13} \cdot e^{\frac{600}{T}}, \qquad (2)$$

$$k_2 = 1.9 \cdot 10^{-33} \cdot e^{\frac{980}{T}} \cdot [M], \qquad (3)$$

$$k_3 = 1 + 1.4 \cdot 10^{-21} \cdot e^{\frac{2200}{T}} \cdot [H_2O]. \qquad (4)$$

[M] and [H_2O] are the local value of air and water vapor molecules in [molec cm^{-3}], respectively. The reaction rate coefficients are from the International Union of Pure and Applied Chemistry (IUPAC) Subcommittee for Gas Kinetic Data Evaluation (http://www.iupac-kinetic.ch.cam.ac.uk/). The photolysis rates are adapted from empirical expressions suggested by Wiegand and Bofinger (2000), which were previously compared with
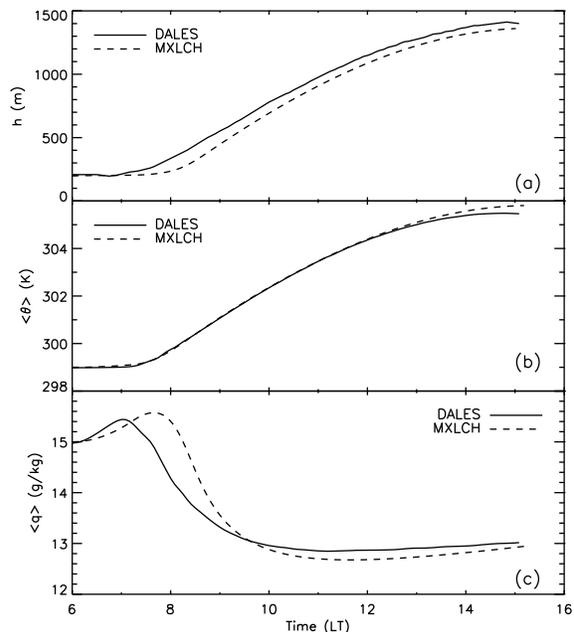

Figure 1: Diurnal evolution of: a) boundary layer height (h), b) ABL-averaged potential temperature ($\langle \theta \rangle$), and c) ABL-averaged specific humidity ($\langle q \rangle$) predicted by DALES and MXLCH.

the Tropospheric Ultraviolet and Visible (TUV) radiation transfer code. Notice that in R17, a variable stoichiometric coefficient n has been introduced to study the sensitivity of the system to the OH-recycling. In the Control case $n = 0$; variations of n are studied and discussed in Section 4.3.

Table 3 outlines the initial profiles and surface fluxes imposed in the Control experiment carried out using both DALES and MXLCH. As mentioned, the time-evolving surface isoprene emission is derived from the 15-day averaged observations as are the initial boundary layer mixing-ratio profiles. It should be noted that chemistry in the Amazonian region is characterized by relatively low levels of NO_x and relatively high surface isoprene emission. Due to the absence of trace species observations above the ABL (a typically difficult observation to obtain), all initial trace species profiles are assumed constant throughout the domain. The sensitivity of the simulation results to these initial profiles are discussed at length in Section 4.. In the LES and MXLCH experiments, mass conservation is preserved within 1%.

3. Evaluation of the numerical experiments

The time evolution of key atmospheric bulk quantities characterizing the simulated Amazonian boundary layer are shown in Figure 1, where, h is the boundary

Number	Reaction			Reaction rate
R1	$O_3 + h\nu$	$\rightarrow$	$O(1D) + O_2$	$6.62 \cdot 10^{-5} \cdot e^{-\frac{0.575}{\cos(\chi)}}$
R2	$O(1D) + H_2O$	$\rightarrow$	$OH + OH$	$1.63 \cdot 10^{-10} \cdot e^{\frac{60}{T}}$
R3	$O(1D) + N_2$	$\rightarrow$	O_3	$2.15 \cdot 10^{-11} \cdot e^{\frac{110}{T}}$
R4	$O(1D) + O_2$	$\rightarrow$	O_3	$3.30 \cdot 10^{-11} \cdot e^{\frac{55}{T}}$
R5	$NO_2 + h\nu$	$\rightarrow$	$NO + O_3$	$1.67 \cdot 10^{-2} \cdot e^{-\frac{0.575}{\cos(\chi)}}$
R6	$CH_2O + h\nu$	$\rightarrow$	HO_2	$5.88 \cdot 10^{-5} \cdot e^{-\frac{0.575}{\cos(\chi)}}$
R7	$OH + CO$	$\rightarrow$	$HO_2 + CO_2$	$2.40 \cdot 10^{-13}$
R8	$OH + CH_4$	$\rightarrow$	CH_3O_2	$2.45 \cdot 10^{-12} \cdot e^{-\frac{1775}{T}}$
R9	$OH + ISO$	$\rightarrow$	RO_2	$1.00 \cdot 10^{-10}$
R10	$OH + MVK$	$\rightarrow$	$HO_2 + CH_2O$	$2.40 \cdot 10^{-11}$
R11	$HO_2 + NO$	$\rightarrow$	$OH + NO_2$	$3.50 \cdot 10^{-12} \cdot e^{\frac{250}{T}}$
R12	$CH_3O_2 + NO$	$\rightarrow$	$HO_2 + NO_2 + CH_2O$	$2.80 \cdot 10^{-12} \cdot e^{\frac{300}{T}}$
R13	$RO_2 + NO$	$\rightarrow$	$HO_2 + NO_2 + CH_2O+ MVK$	$1.00 \cdot 10^{-11}$
R14	$OH + CH_2O$	$\rightarrow$	HO_2	$5.50 \cdot 10^{-12} \cdot e^{\frac{125}{T}}$
R15	$HO_2 + HO_2$	$\rightarrow$	H_2O_2	(see eqs. 1-4)
R16	$CH_3O_2 + HO_2$	$\rightarrow$	PRODUCT	$4.10 \cdot 10^{-13} \cdot e^{\frac{750}{T}}$
R17	$RO_2 + HO_2$	$\rightarrow$	nOH + PRODUCT	$1.50 \cdot 10^{-11}$
R18	$OH + NO_2$	$\rightarrow$	HNO_3	$3.50 \cdot 10^{-12} \cdot e^{\frac{340}{T}}$
R19	$NO + O_3$	$\rightarrow$	$NO_2 + (O_2)$	$3.00 \cdot 10^{-12} \cdot e^{-\frac{1500}{T}}$

Table 2: Chemical reaction scheme used in the numerical experiments of DALES and MXLCH. In the reaction rate functions, T is the absolute temperature and χ is the solar zenith angle. First-order reaction rates are in $[s^{-1}]$ and second-order reactions are in $[cm^3 \, molec^{-1} \, s^{-1}]$. In the Control experiment, $n = 0$ in reaction R17.

layer height, $\langle\theta\rangle$ is the ABL-averaged potential temperature, and $\langle q\rangle$ is the ABL-averaged specific humidity. To maintain consistency with mixed-layer theory, the height of the minimum horizontally-averaged buoyancy flux is taken as the boundary layer height in the LES calculations.

The two models predict similar ABL depth evolution, albeit with the LES code predicting slightly larger boundary layer growth compared to MXLCH. Turbulence is explicitly calculated in the LES and breaks down the temperature inversion at the ABL top 30 minutes prior to MXLCH (i.e., at 0700 LT compared to 0730 LT). In DALES, the entrainment rate (boundary layer growth rate) is a result of the simulations and depends on: 1) the initial profiles (e.g., temperature, wind and moisture), 2) the imposed forcing (e.g., geostrophic wind, surface energy balance, free tropospheric lapse rate), 3) the grid resolution, and 4) the numerical methods used to solve the equations. MXLCH does not explicitly calculate entrainment; rather, it uses a zeroth-order approach to represent entrainment. In MXLCH, the potential temperature jump across the inversion at the ABL top is parameterized as a sharp discontinuity determined by a theoretical and prescribed relationship between entrainment

and surface buoyancy fluxes (β_{MXLCH}); in this study, we assume: β_{MXLCH} = -0.2 (Table 1). This value is larger in magnitude than the value predicted by DALES (where, β_{DALES} averaged between 0800 LT and 1500 LT equaled -0.15). As such, one of the consequences of using the mixed-layer approach is that the larger value of $\beta_{MXLCH} = -0.2$ is compensated by the fact that in the LES entrainment occurs over a larger depth (Pino et al., 2006). To determine the entrainment flux for the other compounds (i.e., specific moisture or reactants), MXLCH assumes that the entrainment flux of each quantity is proportional to the product of the entrainment velocity (the growth rate of the ABL, $\partial h/\partial t$) multiplied by the mixing ratio jump of that quantity across the ABL-FT interface (Vilà-Guerau de Arellano et al., 2009).

Figure 1b reveals the increase of ABL-averaged potential temperature due to heat introduced through surface and entrainment buoyancy fluxes; the time-evolution of $\langle\theta\rangle$ between the models compares well. In contrast, Figure 1c reveals distinct differences in ABL-averaged specific humidity between the models, suggesting that $\langle q\rangle$ is more sensitive to differences in boundary layer growth and FT-ABL exchange than is $\langle\theta\rangle$.

The increased ABL growth predicted by the LES

means: 1) a larger volume into which surface emitted water vapor mixes, and 2) more rapid entrainment of low water vapor mixing ratio air from aloft; both lead to a dilution of the ABL in the LES compared to that in MXLCH during the early morning hours. This dilution process in the LES leads to a smaller ABL-averaged water vapor mixing ratio peak at 0700 LT and to a more rapid rate of decrease of $\langle q \rangle$ in time compared to MXLCH. The MXLCH reproduces the same process, but with a slight time delay. However after 1000 LT, the $\langle q \rangle$-evolution calculated from MXLCH and DALES compare satisfactorily. When analyzing the diurnal evolution of the reactants we will refer to this difference between the LES and MXLCH during the morning transition.

It is important to mention here that we advocate solving dynamics and chemistry simultaneously. We purport that doing so ensures consistency in calculating not only the ABL dilution and FT-ABL exchange rate, but also the absolute temperature and specific humidity which are key variables in the calculation of the reaction rates (Table 2).

The time evolution of isoprene and MVK mixing ratio observed during TROFFEE are used to evaluate the model predictions. The three-dimensional reactant fields calculated by the LES are first horizontally-averaged, and then time-averaged over five minutes. Lastly, the profiles are vertically integrated from the surface to the boundary layer height (defined again as the height of minimum buoyancy flux), which ensures consistency with the assumptions made in MXLCH permitting direct comparison between the two numerical results.

Figure 2 shows the time-evolution of ABL-averaged isoprene (ISO) and MVK. To evaluate the model against the observations, the model results at z = 60 m are used which corresponds to the observation height. Since isoprene is surface-emitted, the largest isoprene gradients are found in the surface layer leading to better agreement with the observations. However, the ABL-averaged isoprene mixing ratio obtained by both simulations agree satisfactorily and reproduce the observed tendency reasonably well; slightly underestimating the 15-day averaged observed isoprene mixing ratio by about 2 to 2.5 [ppbv] during daytime hours.

The models reproduce the observed MVK mixing ratio during the morning hours but then diverge between 1000 and 1400 LT. During this late-morning to midday period, the observations are almost in a steady-state whereas the ABL-averaged MVK mixing ratio increases in the model results. In Section 4., we will analyze and discuss potential reasons for this discrepancy by investigating contributions from a variety of processes and their modulation of MVK diurnal variability. It is also important to note that again, the modeled (lumped) and measured MVK should not agree quantitatively. Also, our
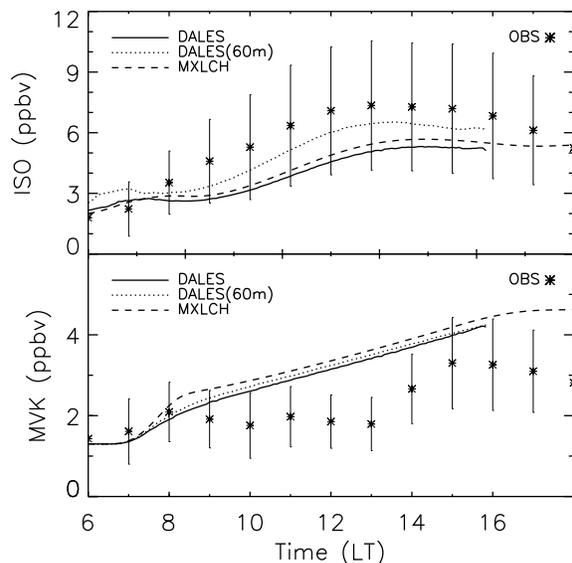

Figure 2: Diurnal evolution of the mixing ratios of: a) isoprene, and b) MVK calculated by DALES and MXLCH and compared against the TROFFEE observations at 60 m. The DALES results correspond to ABL-averaged values. The results labeled by DALES(60m) are horizontally-averaged 60 m values from DALES at the same height as the TROFFEE measurements. The observations have been averaged over 15 days (14-29 September 2004). The error bars represent the standard deviation.

numerical experiments have ignored some key processes; dry and wet deposition, for instance.

The time-evolution of the ABL-averaged ISO and MVK values calculated by the two different numerical techniques (DALES and MXLCH) also agree reasonably well. Explicit calculation of the intensity of segregation (defined as: $I_s = \frac{\overline{a'b'}}{\overline{a}\,\overline{b}}$, the ratio of the covariance of species to the product of the horizontal averages where an instantaneous quantity $a = \overline{a} + a'$, e.g., Schumann, 1989) from DALES reveals that $I_s < 1\%$ for the most potentially sensitive reactions being considered (R9 and R19, see Table 2). I_s values less than 1% indicates efficient reactant mixing, which suggests MXLCH's instantaneous and homogeneous mixing assumption is reasonable for the chemical mechanism and the uniformly imposed surface source distribution considered here. Vilà-Guerau de Arellano et al. (1990), Krol et al. (2000) and Patton et al. (2001) showed that negative I_s values are expected when the species are not-premixed and when species are emitted non-uniformly in space (i.e., plume emission, heterogeneous surfaces, or intermittent canopy emissions). These findings there-

	O_3	NO	NO_2	ISO	MVK	CH4	CO
Initial scalar value: [ppbv]							
z < 200.0 m	10.0	0.0	1.0	2.0	1.3	1724.	124.
200.0 m > z < 212.5 m	10.0	0.0	0.0	2.0	1.3	1724.	124.
z > 212.5 m	10.0	0.0	0.0	2.0	1.3	1724.	124.
Surface emission flux [ppbv m s^{-1}]	0.0	$5 \cdot 10^{-4}$	0.0	$0.65 \cdot e^{(-\zeta^2/2)}$	0.0	0.0	0.0

Table 3: Initial mixing ratio [ppbv] and surface emission fluxes [ppbv m s^{-1}] of the reactive species prescribed in the numerical experiments using the large-eddy simulation technique (DALES) and the mixed layer model (MXLCH). Reactants in Table 2 that are not included in the table have zero initial concentrations and zero surface emissions. For the molecules O_2 and N_2 we have imposed the values $2 \cdot 10^8$ and $8 \cdot 10^8$ [ppbv] respectively. For the surface emission of isoprene the ζ-function is $\zeta = ((t + 18000) - 42705)/7999$ with a conversion factor from [ppbv m s^{-1}] to [mg m^{-2} hr^{-1}] equal to 11.5. This function has been fitted to the TROFFEE isoprene observations emissions averaged during the period 14-29 September 2004. t is the local time in [s]. No deposition fluxes are imposed.
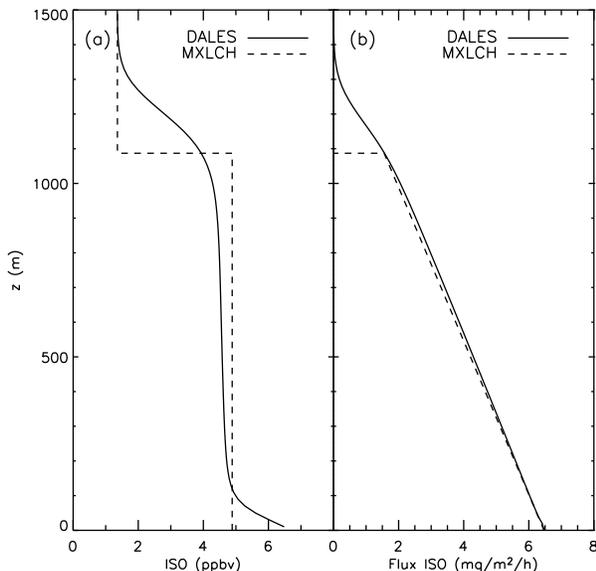

Figure 3: One-hour averaged vertical profiles of isoprene mixing ratio and vertical isoprene flux calculated with DALES and the MXLCH model at 1200 LT. For the MXLCH model, we use the values calculated at the entrainment zone and at the mixed-layer and assume a linear profile.

fore disagree with those who purport using intensity of segregation to explain high OH-observations in tropical forests (*e.g.,* Butler et al., 2008; Pugh et al., 2009).

To complete the intercomparison, Figures 3 and 4 show DALES and MXLCH predicted vertical profiles of isoprene and nitric oxide (NO) mixing ratio and flux at 1200 LT. The mixing ratio profiles (Figures 3a and 4a) are remarkably well reproduced in the region from 100 m $\leq$ z $\leq$ 900 m, *i.e.,* the mixed layer. The surface layer (z $\leq$ 100 m) and entrainment zone (900 m $\leq$ z $\leq$ 1500 m)

reveal strong ISO- and NO-vertical gradients in the LES; these gradients are not reproduced by MXLCH. These differences result from MXLCH's assumption that the ABL mixes perfectly, while DALES solves the full set of filtered non-linear equations governing the interactions between dynamics and chemistry and is therefore able to simulate the non-linear behavior near the interfaces.

The ISO- and NO-flux profiles predicted by the LES versus MXLCH reveal a different behavior with height (Figures 3b and 4b). The vertical isoprene flux profile is linear with height indicating that the chemical term in the conservation equation for vertical isoprene flux is small compared to the transport terms (Gao and Wesely, 1994; Vinuesa and Vilà-Guerau de Arellano, 2003); *i.e.,* for isoprene, the turbulent mixing time scale is smaller than the chemical reaction time scale. In contrast, the one-hour averaged NO-flux profile calculated by DALES departs from linearity. This departure is most notable near the interfaces with the surface and the entrainment zone, where NO chemistry is more rapid than the turbulent mixing process. As shown by Figure 4b this non-linear behavior is not reproduced by the mixed-layer model since it assumes a linear flux profile for all species. NO measurements taken within the atmospheric surface layer (z $\leq \sim$100 m) are clearly influenced by chemistry as indicated by the large curvature of the NO-flux profile (Gao and Wesely, 1994).

Although predictions using these numerical methods differ in these ways, this comparison corroborates the overall suitability of MXLCH to reproduce mixed-layer quantities as was previously shown when discussing Figure 2. It is important to emphasize that compared to typical box-model chemistry studies (where turbulence and entrainment are generally ignored), MXLCH incorporates the coupling between atmospheric dynamics and chemistry associated with a convective boundary layer and its diurnal variation while retaining much of a box
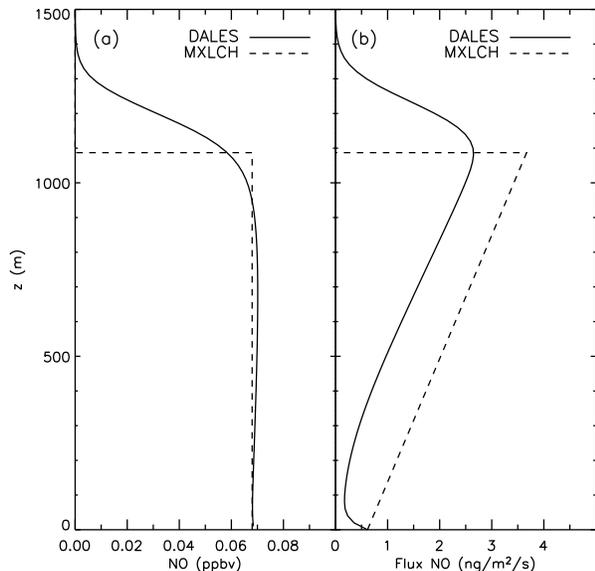
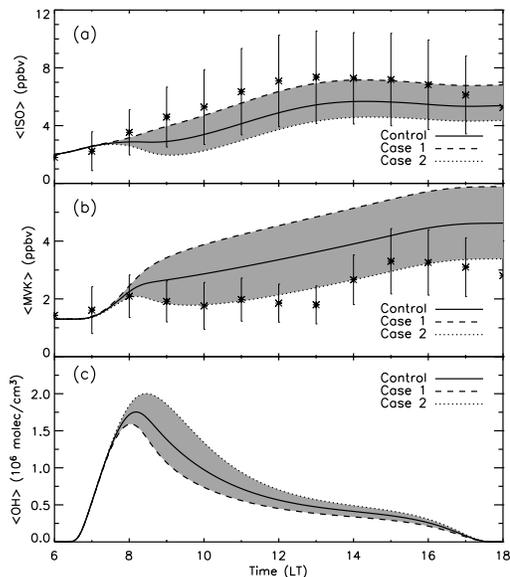Figure 4: Same as Figure 3 but for nitric oxide (NO).

Figure 5: Diurnal evolution of: (a) isoprene, and (b) MVK mixing ratio from MXLCH compared against the TROFFEE observations at 60 m. The MXLCH OH concentration is shown in (c). The shaded regions show the model sensitivity to the initial isoprene and MVK mixing ratio jump between the mixed layer and the FT. The shaded region marks the range of possible predicted values to variations in entrainment discussed here. The continuous, dashed, and dotted lines correspond to the Control Case, Case 1, and Case 2, respectively. The observations have been averaged over 15 days (14-29 September 2004) and the error bars depict the standard deviation.

model's simplicity.

4. Processes determining the time evolution of ABL-averaged species

The model/observation intercomparison presented in Section 3. provides sufficient confidence to embark upon a systematic sensitivity study using MXLCH to investigate factors affecting the uncertainties seen in the measurements. An important factor is the role of exchange between the free troposphere and the ABL in determining the diurnal variability of ABL-averaged isoprene, MVK and OH. This sensitivity study will also answer the question whether the diurnal variability of ABL-averaged isoprene imposed by isoprene entrainment is of similar magnitude to variations in isoprene and NO surface emissions.

Table 4 outlines the parameter space variations investigated (*i.e.,* variations in initial concentration profiles and surface emission fluxes). Only one parameter type is changed for a particular case and each case is compared against the Control case described in Tables 1 and 3.

4.1 Exchange between the ABL and the overlying FT

The first of these numerical experiments is designed to show the impact of species entrainment on the diurnal evolution of ABL-averaged reactants; compared to the Control case, Case 1 implements a higher FT ISO and MVK mixing ratio at 0500 LT, while Case 2 prescribes

lower FT ISO and MVK mixing ratio at 0500 LT. Notice that for these two cases we change simultaneously two conditions since ISO and MVK have similar evolutions.

Compared to the Control case, Case 1 imposes higher isoprene levels in the residual layer/free troposphere while keeping ABL isoprene levels the same. This case is inspired by early measurements (Zimmerman et al., 1988) that showed high isoprene levels above the boundary layer in the early morning, a situation which is conceivable over the relatively unpolluted (low NO_x) Amazonian region (nighttime NO_3 chemistry would act to diminish isoprene aloft were this to be a polluted region). As the ABL begins to grow during the morning transition, isoprene-rich air is entrained into the ABL. Contrast this with the morning transition for Case 2 where very low isoprene mixing ratio air (*i.e.,* 0 [ppbv]) is entrained into the ABL from aloft.

The diurnal evolution of bulk ISO, MVK mixing ratio and the OH concentration further emphasizes the importance of FT-ABL exchange (Figure 5); this figure shows

Initial concentration profile variations ($z > 212.5$ m) [ppbv]

	O_3	NO	NO_2	ISO	MVK	CH4	CO
Control	10.0	0.0	0.0	2.0	1.3	1724.0	124.0
Case 1	10.0	0.0	0.0	**4.0**	**2.6**	1724.0	124.0
Case 2	10.0	0.0	0.0	**0.0**	**0.0**	1724.0	124.0

Surface emission flux variations [ppbv m s^{-1}]

	O_3	NO	NO_2	ISO	MVK	CH4	CO
Control	0.0	$5 \cdot 10^{-4}$	0.0	$0.65 \cdot e^{(-\zeta^2/2)}$	0.0	0.0	0.0
Case 3	0.0	$5 \cdot 10^{-4}$	0.0	$\mathbf{0.88} \cdot e^{(-\zeta^2/2)}$	0.0	0.0	0.0
Case 4	0.0	$5 \cdot 10^{-4}$	0.0	$\mathbf{0.42} \cdot e^{(-\zeta^2/2)}$	0.0	0.0	0.0
Case 5	0.0	$\mathbf{5 \cdot 10^{-3}}$	0.0	$0.65 \cdot e^{(-\zeta^2/2)}$	0.0	0.0	0.0
Case 6	0.0	**0.0**	0.0	$0.65 \cdot e^{(-\zeta^2/2)}$	0.0	0.0	0.0

Table 4: Initial mixing ratio [ppbv] and surface emission fluxes [ppbv m s^{-1}] of the reactive species prescribed in the MXLCH parameter space experiments; the bold values indicate the parameters modified for each experiment.

the Control case compared with Cases 1 and 2. For ISO (Figure 5a), the dashed line shows the enhancement of isoprene mixing ratio resulting from entrainment of isoprene rich air (Case 1). The dotted line shows the dilution of ABL-averaged isoprene mixing ratio resulting from entrainment of isoprene-poor air from aloft (Case 2). As a consequence, when the convectively driven ABL growth begins at 0800 LT, $\langle ISO \rangle$ and $\langle MVK \rangle$ both depart significantly from the Control case. The magnitude of the modulation is proportional to the initial isoprene mixing ratio jump across the FT-ABL interface.

In Figure 5, variations in entrainment produce variations in predicted $\langle ISO \rangle$ and $\langle MVK \rangle$ mixing ratios that generally encapsulate the observations; recall that measured and modeled MVK should not agree quantitatively. These variations of $\langle ISO \rangle$ and $\langle MVK \rangle$ mixing ratios due solely to entrainment support our suggestion that properly accounting for entrainment is an $\mathcal{O}(1)$ effect when discussing diurnal variations of surface layer chemistry.

The ABL-averaged hydroxyl radical concentration ($\langle OH \rangle$) is also sensitive to the sign and magnitude of FT-ABL exchange (Figure 5c). In Case 1, entrainment increases ABL-averaged isoprene and MVK mixing ratio, $\langle OH \rangle$ thereby decreases by about 22% at 1000 LT. For Case 2, the $\langle OH \rangle$ concentration increases 39% at 1000 LT due to entrainment of isoprene- and MVK-poor air originating above the boundary layer in the overlying residual layer or free troposphere. The $\langle OH \rangle$ concentration peak at approximately 0800 LT occurs largely because isoprene emissions are still small during the early morning hours (sunrise is at 0600 LT) suggesting that in these early morning hours, isoprene chemistry is insufficient to deplete OH formed by photochemistry.

A combination of the inversion strength at the top of the boundary layer and the imposed surface buoyancy flux forcing the convection could also control the $\langle OH \rangle$ peak. To determine the sensitivity of this $\langle OH \rangle$-peak to the inversion strength, we carried out a separate experiment increasing the potential temperature gradient across the inversion (the inversion strength) from $\Delta \theta = 1$ K (Control case, Table 1) to $\Delta \theta = 4$ K (not shown). Keeping all other forces the same, an increase in $\Delta \theta$ delays and reduces the growth rate of the ABL and the entrainment of FT air into the ABL. In this experiment where $\Delta \theta$ increases to 4 K, the $\langle OH \rangle$ maximum increases by 24% and is delayed by 30 minutes compared to the Control case. For surface emitted species, the reduced exchange between the free troposphere and the ABL enhances ABL mixing ratios of those species, which yields higher OH-concentrations as the sun rises and photolysis reactions become important. In addition to this dynamical process, the timing of the $\langle OH \rangle$-peak is also very sensitive to the onset of isoprene emission occurring during the morning transition from stable to unstable stratification.

These simulations emphasize the need to obtain information regarding the vertical variation of reactants during the morning transition to assess the impact of entrainment on mixed-layer species. Therefore in order to accurately predict diurnal mixed-layer reactant evolution, we strongly advocate for profile observations (within the boundary layer up to heights above the mixed-layer) of mean thermodynamic and reacting variables on tall towers or via tethered balloon.

4.2 Surface emissions

An important question arises after discussing the role of the FT-ABL exchange on the ISO, MVK and OH-diurnal variability: What is the relative importance of surface emission to entrainment of FT air in determining
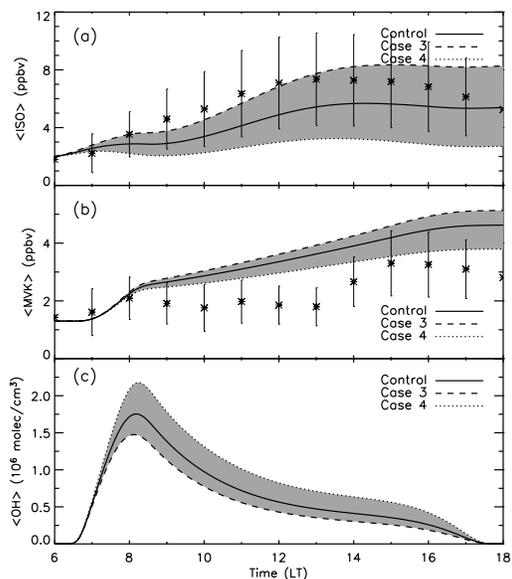
Figure 6: Same as Figure 5, but for ± 35% variation in surface isoprene emission, *i.e.,* Control case, Case 3, and Case 4.

Figure 7: Same as Figure 5, but for variations in surface NO emission, *i.e.,* Control case, Case 5, and Case 6.

observed near-surface concentrations? To address this question, in this second experiment Case 3 (Case 4) imposes a 35% larger (smaller) surface isoprene emission flux than the Control case, respectively; this percentage is similar to the variability found in the isoprene surface measurements (Karl et al., 2007). Cases 5 and 6 test surface emissions, but investigate the influence of NO emission variations.

All else held constant, the diurnal variability of ⟨ISO⟩, ⟨MVK⟩ and ⟨OH⟩ reveals a significant influence from variations in the magnitude of the surface isoprene flux (Figure 6). A 35% isoprene emission increase (Case 3, dashed line) leads to an increase of ABL-averaged ISO (34% increase at 1000 LT), which yields increases in ⟨MVK⟩ (6% increase at 1000 LT) and depletes ⟨OH⟩ (26% decrease at 1000 LT). Lower isoprene emissions (Case 4, dotted line) produces the opposite behavior; namely, a 33% decrease, 9% decrease, and 35% increase at 1000 LT for ISO, MVK and OH, respectively. Comparing the shaded regions of Figures 5 and 6, we find that entrainment and surface emissions can have equal influence on ABL-averaged concentrations.

This result has repercussions for regional scale isoprene studies. It is common practice when modeling isoprene at larger scales to reduce isoprene emission levels up to 50% in order to obtain agreement with OH observations (*e.g.,* Ganzeveld et al., 2008). The analysis presented here shows that FT-ABL exchange driven by the dynamic growth of the ABL (*i.e.,* entrainment) and the reactant's initial distribution at sunrise has similar influ-
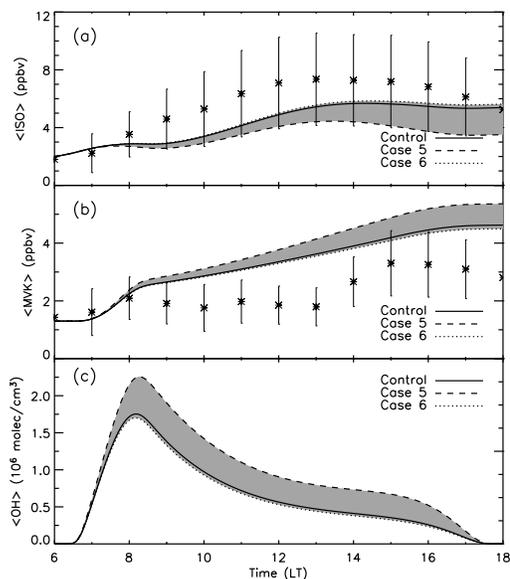
ence as surface emission. Therefore, we purport that improper representation of entrainment in these large-scale chemistry-transport models could explain much of the OH disagreement.

The daily evolution of ⟨ISO⟩, ⟨MVK⟩ and ⟨NO⟩ is also sensitive to surface NO emission variations (Figure 7). A factor of ten increase in surface NO emission (Case 5, dashed line) yields a 46% increase in daytime OH due to increased production of ozone during the day (at 1800 LT the ozone mixing ratio in the Control and Case 5 is 18.0 [ppbv] and 22.4 [ppbv], respectively). Notice how the ⟨OH⟩ increase gradually decreases the isoprene levels through out the day (via R9) and increases ⟨MVK⟩ levels (mainly through R13). Completely eliminating the surface NO flux (Case 6, dotted line) does not significantly influence the results, which suggest that most NO in the Control case is produced through photo-dissociation of NO_2.

4.3 Chemical pathways

Recent literature has suggested a OH recycling pathway for low NO_x conditions (*e.g.,* Lelieveld et al., 2008; Butler et al., 2008; Pugh et al., 2009; Peeters et al., 2009). To investigate whether recycling of OH has an impact on isoprene, MVK and OH, modifications to R17 have been suggested.

To demonstrate the importance of using an appropriate ABL dynamics parameterization when studying new OH chemical pathways, following Lelieveld et al. (2008) we perform a sensitivity analysis by modifying R17 to
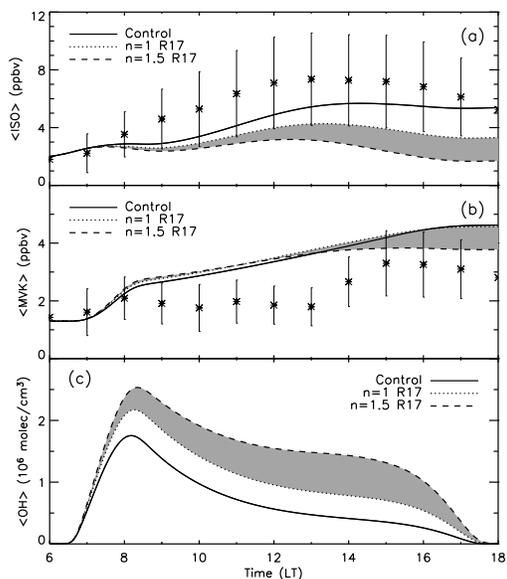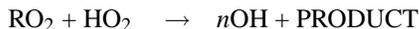
Figure 8: Sensitivity of MXLCH predictions of ABL-averaged isoprene, MVK and OH evolution to variations of R17 and its ability to produce OH. The three cases presented vary the stoichiometric coefficient n in R17 (see Table 2); where, $n = 0$ (solid line), $n = 1$ (dashed line), or $n = 1.5$ (dotted line). The shaded region depicts the range of MXLCH predictions to these variations of n.
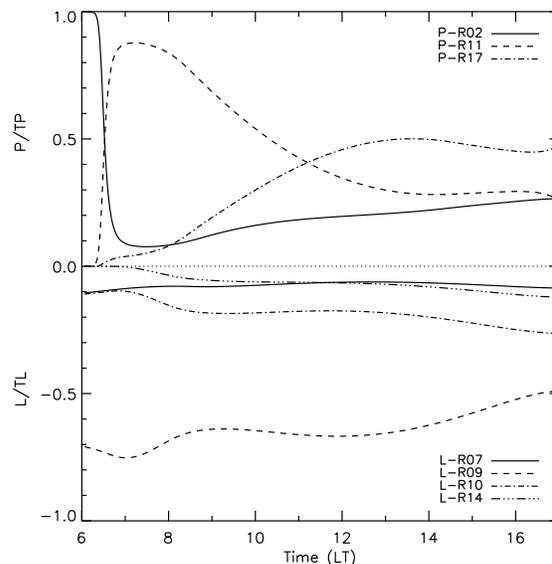

Figure 9: Time evolution of the chemical production (P, positive values) and loss (L, negative values) terms involved in the conservation equation for OH when $n = 1.5$ in reaction R17. The terms are made non-dimensional by the total production (TP) and loss (TL). For clarity, the loss reactions R8, R10, and R18 are not shown since they cumulatively contribute less than 10% to the total OH reactivity.

appear as:

$$RO_2 + HO_2 \quad \rightarrow \quad nOH + PRODUCT$$

where, chemical processing of RO_2 and HO_2 now yields OH at a rate equal to $1.50 \cdot 10^{-11}$ [molec cm^{-3}], with a stoichiometric coefficient n equal to 0, 1, or 1.5. As expected, OH-production increases dramatically for both $n = 1$ and $n = 1.5$ (Figure 8); at 1200 LT, the OH concentration is $1.0 \cdot 10^6$ [molec cm^{-3}] and $1.6 \cdot 10^6$ [molec cm^{-3}], respectively. The increased OH subsequently depletes ISO to unrealistic levels for Amazonia. This OH increase is not uniform through the day, where a post-sunrise OH maximum is controlled by the morning evolution of the ABL's thermodynamic characteristics and the subsequent influence of boundary layer growth on FT-ABL exchange, and also by the onset of isoprene surface emission.

The chemical production and loss terms in the conservation equation for OH provide further evidence for the importance of boundary layer dynamics and entrainment on OH reactivity. Figure 9 presents the chemical production (P) and loss (L) terms normalized by the total production (TP) or loss (TL) for the case where $n = 1.5$ in reaction R17; only loss reactions with larger than 10% contribution are shown. Notice that the production terms are

sensitive to the boundary layer and UV-B radiation evolution. The morning OH maximum (*i.e.,* between 0600 and 0900 LT) is clearly dominated by OH produced by R11. As discussed in Section 4.1, the magnitude of this peak depends on the evolution of both thermodynamics and chemistry during the morning transition. Near 1200 LT when isoprene emissions are maximized, R17 also generates a second OH maximum due to increased RO_2 production. In contrast to production, the loss reactions reveal very little diurnal variability and are dominated by OH destruction through reactions with isoprene and MVK.

5. The relationship between surface isoprene flux and its concentration

Extending our findings in Sections 3. and 4. to a wider range of isoprene surface emissions, we now incorporate additional observations from: 1) Kuhn et al. (2004) in the Amazon, 2) the AMAZE-08 campaign (Karl et al., 2009) also in the Amazon, and 3) Karl et al. (2009) over a Costa Rican (CR) rain forest. By so doing, one can estimate the combined role of FT-ABL exchange, surface emission and OH reactivity on isoprene mixing ratios above tropical rain forests.
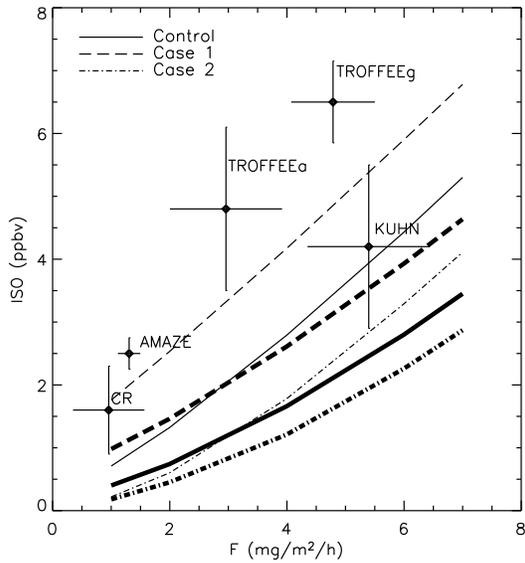
Figure 10: Observations and model results showing the relationship between the surface isoprene flux (F) and mixing ratio (ISO) at 1200 LT. The model results correspond to the experiments shown in Figure 3 (thin lines) and to results using the new reaction R17 with $n = 1.5$ (thick lines). The observations presented include: TROFFEE surface (TROFFEEg), TROFFEE upper air (TROFFEEa), AMAZE-08, Khun, and Costa Rica (CR); the observations include their standard deviations.

Figure 10 shows one-hour averaged surface isoprene emissions versus isoprene mixing ratio for these observations and for MXLCH, where we focus on one-hour averages valid at 1200 LT. To calculate the MXLCH results, we use the dynamical and chemical conditions for three of the cases previously discussed: Control case, Case 1 and Case 2 (Table 4), and then each of these cases is repeated with midday surface isoprene emissions varying from 1 to 8 [mg m^{-2} hr^{-1}]. The difference between the thin and thick lines in Figure 10 arises from R17; where, the thin lines are calculated with $n = 0$ and the thick with $n = 1.5$. Two important points come from this figure: 1) differences in the chemical mechanism (*i.e., n = 0* or $n = 1.5$ in R17) determines the mean slope and curvature of the line relating surface isoprene flux and isoprene mixing ratio, and 2) the intercept with the ordinate varies with the importance of entrainment (*i.e.,* FT-ABL exchange); displacement of the intercept can determine whether we find satisfactory agreement between observed surface emission and its respective mixing ratio evolution. Entrainment apparently plays as substantial a role as either surface emission or chemical pathway when interpreting the observations. In closing, it is also important to mention that additional OH recycling yields

relatively low isoprene mixing ratio which has not been observed in the measurements above the tropical forests.

6. Conclusions

The daily cycle of isoprene, methyl-vinyl-ketone and the hydroxyl radical in the Amazonian basin is studied through a combination of observations and numerical experiments. Emphasis is placed on using an approach which incorporates a balance of the essential boundary layer dynamics and the essential chemical reactions of the O_3-NO_x-VOC-HO_x system. By doing so we are able to reproduce and study key contributions to the isoprene budget and their impact on diurnal variability of isoprene and other related species.

We conclude that the FT-ABL exchange (entrainment) is as important as the surface isoprene emission in determining isoprene mixing ratios. The FT-ABL exchange is controlled by the evolution of boundary layer dynamics, the vertical structure of temperature and moisture, and by the initial mixing ratio of isoprene in and above the atmospheric boundary layer at sunrise. Comparisons with the 15-day average mixing ratio observations suggest that the noon-time behavior of ISO and MVK is dependent on the FT-ABL exchange of these two reactants. By combining measurements from widely varying observational campaigns with numerical experiments, the relationship between surface isoprene emission and isoprene mixing ratio is further studied; at noon, we find a relationship between these variables where the mean slope and curvature are determined by the chemical mechanism and the intercept is dependent on the FT-ABL exchange. Sensitivities of ABL-averaged OH to an OH recycling mechanism are also discussed, where significant recycling of OH is found to deplete ISO to unrealistic levels for Amazonia and to produce an asymmetric diurnal OH evolution which is tied to the morning evolution of the ABL and the timing of isoprene surface emission.

These numerical results demonstrate the ability of large-eddy simulation in studying the interplay between boundary layer processes and complex chemistry. Key processes in the O_3-NO_x-VOC-HO_x system (like dry deposition which depends on the magnitude of the reactant flux divergence, boundary layer cloud venting and surface heterogeneity effects) still remain to be investigated with systematic LES experiments in concert with available and forthcoming measurements.

As a tool that sits between box models and turbulence-resolving LES, a mixed-layer model coupled to a chemical solver can serve as a very useful instrument to analyze observations taken during convective diurnal conditions. Because the mixed-layer model makes similar assumptions to those made in parameterizations which are currently implemented in larger-scale chemistry-transport

models to represent turbulence/chemistry interactions, our results point to the need to revisit the parameterizations of FT-ABL exchange and their impact on reactant diurnal variability. As such, MXLCH results can be used to support the interpretation of more complex chemistry-transport models.

REFERENCES

Betts, A. K. and C. Jacob, 2002: Evaluation of the diurnal cycle of precipitation, surface thermodynamics, and surface fluxes in the ECMWF model using LBA data, *J. Geophys. Res.*, **107**, DOI20,8045.

Butler, T., D. Taraborrelli, C. Brühl, H. Fischer, H. Harder, M. Martinez, J. Williams, M. Lawrence, and J. Lelieveld, 2008: Improved simulation of isoprene oxidation chemistry with the ECHAM5/MESSy chemistry climate-model: lessons from the GABRIEL airborne field camapign, *Atmos. Chem. Phys.*, **8**, 4259–4546.

Casso-Torralba, P., J. Vilà-Guerau de Arellano, F. Bosveld, M. Soler, A. Vermeulen, C. Werner, and E. Moors, 2008: Diurnal and vertical variability of the sensible heat and carbon dioxide budgets in the atmospheric surface layer, *J. Geophys. Res.*, **113**, D12119.

Conzemius, R. and E. Fedorovich, 2006: Dynamics of sheared convective boundary layer entrainment. Part II: Evaluation of bulk model predictions of entrainment flux, *J. Atmos. Sci.*, **63**, 1179–1199.

Davis, K. J., D. H. Lenschow, and P. R. Zimmerman, 1994: Biogenic nonmethane hydrocarbon emissions estimated from tethered ballon observations, *J. Geophys. Res.*, **99**, 25587–25598.

Fan, S.-M., S. C. Wofsy, P. S. Bakwin, D. J. Jacob, and D. R. Fitzjarrald, 1990: Atmosphere-biosphere exchange of CO_2 and O_3 in the central Amazon forest, *J. Geophys. Res.*, **95, D10**, 16851–16864.

Fuentes, J. D., M. Lerdau, R. Atkinson, D. Baldocchi, J. W. Bottenhiem, P. Ciccioli, B. Lamb, C. Geron, L. Gu, A. Guenther, T. D. Sharkey, and W. Stockwell, 2000: Biogenic hydrocarbons in the atmospheric boundary layer: A review, *Bulletin Amer. Meteor. Soc.*, **81**, 1537–1575.

Ganzeveld, L., G. Eerdekens, G. Feig, H. Fisher, H. Harder, R. Konigstedt, D. Kubistin, M. Martinez, F. X. Meiner, H. A. Scheeren, V. Sinha, D. Taraborrelli, J. Williams, J. Vilà-Guerau de Arellano, and J. Lelieveld, 2008: Surface and boundary layer exchanges of volatile organic compounds, nitrogen dioxides and ozone during the GABRIEL campaign, *Atmos. Chem. Phys.*, **8**, 6223–6224.

Gao, W. and M. L. Wesely, 1994: Numerical modelling of the turbulent fluxes of chemically reactive trace gases in the atmospheric boundary layer, *J. Appl. Meteorol.*, **33**, 835–847.

Garstang, M., S. Ulanski, S. Greco, J. Scala, R. Swap, D. Fitzjarrald, D. M. E. Browell, M. Shipman, V. Connors, R. Harriss, and R. Talbot, 1990: The Amazon Boundary-Layer Experiment ABLE 2B: A meteorlogical perspective, *Bulletin Amer. Meteor. Soc.*, **71**, 19–32.

Guenther, A., P. Zimmerman, L. Klinger, J. Greenberg, C. Ennis, H. Westberg, G. Allwine, and C. Geron, 1996: Estimates of regional natural volatile organic compound fluxes from enclosure and ambient measurements, *J. Geophys. Res.*, **101**, 1345–1359.

Heus, T., C. C. van Heerwaarden, H. J. J. Jonker, A. P. Siebesma, S. Axelsen, K. van den Dries, O. Geoffroy, A. F. Moene, D. Pino, S. R. de Roode, and J. Vilà-Guerau de Arellano, 2010: Formulation and numerical studies by the Dutch Atmospheric Large-Eddy Simulation (DALES), *Geosci. Model Dev. Discuss.*, **3**, 99–180.

Jonker, H. J. J., P. G. Duynkerke, and J. W. M. Cuijpers, 1999: Mesoscale fluctuations in scalars generated by boundary layer convection, *J. Atmos. Sci.*, **55**, 801–808.

Karl, T., A. Guenther, A. Turnipseed, P. Artaxo, and S. T. Martin, 2009: Rapid formation of isoprene photo-oxidant products observed in Amazonia: Chemistry, and transport of biogenic volatile organic compounds in the lower atmosphere over Amazonia, *Atmos. Chem. Phys.*, **9**, 7753–7769.

Karl, T., A. Guenther, R. J. Yokelson, J. Greenberg, M. Potosnak, D. R. Blake, and P. Artaxo, 2007: The

tropical forest and fire emissions experiment: Emission, chemistry, and transport of biogenic volatile organic compounds in the lower atmosphere over Amazonia, *J. Geophys. Res.*, **112, D18**, 302.

Keller, M., D. J. Jacob, S. C. Wofsy, and R. C. Harriss, 1991: Effects of tropical deforestation on global and regional atmospheric chemistry, *Climactic Change*, **19, 1-2**, 139–158.

Krol, M. C., M. J. Molemaker, and J. Vilà-Guerau de Arellano, 2000: Effects of turbulence and heterogeneous emissions on photochemically active species in the convective boundary layer, *J. Geophys. Res.*, **105**, 6871–6884.

Kuhn, U., S. Rottenberger, T. Biesenthal, A. Wolf, G. Schebeske, P. Ciccioli, E. Brancaleoni, M. Frattoni, T. Tavares, and J. Kesselmeier, 2004: Seasonal differences in isoprene and light-dependent monoterpene emission by Amazonian tree species, *Glob. Change Biol.*, **10**, 663–682.

Lelieveld, J., T. M. Butler, J. N. Crowley, T. J. Dillon, H. Fischer, L. Ganzeveld, H. Harder, M. G. Lawrence, M. Martinez, D. Taraborrelli, and J. Willimas, 2008: Atmospheric oxidation capacity sustained by a tropical forest, *Nature*, **452**, 737–740.

Lilly, D. K., 1968: Models of cloud-topped mixed layers under s strong inversion, *Quart. J. Roy. Meteorol. Soc.*, **94**, 292–309.

Martin, C. L., D. Fitzjarrald, M. Garstang, A. P. Oliveira, S. Greco, and E. Brodwell, 1988: Structure and growth of the mixing layer over the Amazonian rain forest, *J. Geophys. Res.*, **93**, 1361–1375.

Patton, E. G., K. J. Davis, M. C. Barth, and P. P. Sullivan, 2001: Decaying scalars by a forest canopy: A numerical study, *Bound.-Layer Meteorol.*, **100**, 91–129.

Peeters, J., T. L. Nguyen, and L. Vereecken, 2009: HO$_x$ radical regeneration in the oxidation of isoprene, *Phys. Chem. Chem. Phys.*, **11**, 5953–5939.

Pino, D., J. Vilà-Guerau de Arellano, and P. G. Duynkerke, 2003: The contribution of shear to the evolution of a convective boundary layer, *J. Atmos. Sci.*, **60**, 1913–1926.

Pino, D., J. Vilà-Guerau de Arellano, and S. W. Kim, 2006: Representing shear convective boundary layer by zeroth- and first-order jump mixed layer models: Large-eddy simulation verification, *J. Appl. Meteorol.*, **45**, 1224–1243.

Pugh, T. A. M., A. R. MacKenzie, C. N. Hewitt, B. Langford, P. M. Edwards, K. L. Furneaux, D. E. Heard, J. R. Hopkins, C. E. Jones, A. Karunaharan, J. Lee, G. Mills, P. Misztal, S. Moller, P. S. Monks, and L. K. Whalley, 2009: Simulating atmospheric composition over South-East Asian tropical rainforest: Performance of a chemistry box model, *Atmos. Chem. Phys. Discuss.*, **9**, 19243–19278.

Schumann, U., 1989: Large-eddy simulation of turbulent diffusion with chemical reactions in the convective boundary layer, *Atmos. Environ.*, **23**, 1713–1729.

Sullivan, P. P., C. Moeng, B. Stevens, D. H. Lenschow, and S. D. Mayor, 1998: Structure of the entrainment zone capping the convective atmospheric boundary layer, *J. Atmos. Sci.*, **55**, 3042–3064.

Tennekes, H., 1973: A model for the dynamics of the inversion above a convective boundary layer, *J. Atmos. Sci.*, **30**, 558–567.

Tuazon, E. C. and R. Atkinson, 1990: A product study of the gas-phase reaction of Isoprene with the OH radical in the presence of NOx, *Int. J. Chem. Kinet.*, **22, 12**, 1221–1236.

van Heerwaarden, C. C., J. Vilà-Guerau de Arellano, A. F. Moene, and A. A. M. Holtslag, 2009: Interactions between dry-air entrainment, surface evaporation and convective boundary layer development, *Quart. J. Roy. Meteorol. Soc.*, **135**, 1277–1231.

Verwer, J. G., 1994: Gauss Seidel iterations for stiff ODEs from chemical kinetics, *SIAM J. Sci. Comput.*, **15**, 1243–1250.

Verwer, J. G. and D. Simpson, 1995: Explicit methods for stiff ODEs from atmospheric chemistry, *Appl. Numer. Math.*, **18**, 413–430.

Vilà-Guerau de Arellano, J., B. Gioli, F. Miglietta, H. Jonker, H. Baltink, R. Hutjes, and A. Holtslag, 2004: Entrainment process of carbon dioxide in the atmospheric boundary layer, *J. Geophys. Res.*, **109**, D18110.

Vilà-Guerau de Arellano, J., S. Kim, M. C. Barth, and E. G. Patton, 2005: Transport and chemical transformations influenced by shallow cumulus over land, *Atmos. Chem. Phys.*, **5**, 3219–3231.

Vilà-Guerau de Arellano, J., A. M. Talmon, and P. J. H. Builtjes, 1990: A chemically reactive plume model for the NO-NO$_2$-O$_3$ system, *Atmos. Environ.*, **24**, 2237–2246.

Vilà-Guerau de Arellano, J., K. van den Dries, and D. Pino, 2009: On inferring isoprene emission surface flux from atmospheric boundary layer concentration measurements, *Atmos. Chem. Phys.*, **9**, 3629–3640.

Vinuesa, J. F. and J. Vilà-Guerau de Arellano, 2003: Fluxes and (co-)variances of reacting scalars in the convective boundary layer, *Tellus B*, **55**, 935–949.

Wiegand, A. N. and N. D. Bofinger, 2000: Review of empirical methods for the calculation of the diurnal N_2O photolysis reaction rate, *Atmos. Environ.*, **34**, 99–108.

Yokelson, R. J., T. J. Christian, T. G. Karl, and A. Guenther, 2008: The tropical forest and fire emissions experiment: labarotory fire measurements and synthesis of the campaign data, *Atmos. Chem. Phys.*, **8**, 3509–3527.

Zimmerman, P. R., J. P. Greenberg, and C. E. Westberg, 1988: Measurement of atmospheric hydrocarbons and biogenic emission fluxes in the Amazon boundary layer, *J. Geophys. Res.*, **93**, 1407–1416.